Superconducting Vortex Matter Under Extreme Confinement: The Effect Of Anisotropic Interaction

Lihao Yan and Advisor: Boldizsár Jankó

University of Notre Dame

(Dated: April 6, 2021)

Abstract

Most novel superconductors are expected to show unconventional pairing and anisotropic vortex-vortex interaction. However, it is notoriously difficult to provide experimental evidence for the presence of anisotropic interaction. In this project we investigate superconducting vortex matter under the extreme confinement of nanoscale and mesoscopic samples. We calculate numerically the structure of Abrikosov vortices trapped in mesoscopic samples with a variety of rotational symmetry, such as triangles, squares, disks, etc. We use a combination of numerical techniques, such as energy landscape investigation via the eigenvector following method, and self-consistent numerical Ginzburg Landau calculations. We find that the interplay between sample geometry and vortex interaction anisotropy can qualitatively alter the structure of vortex matter under this extreme confinement regime. We argue that containers with low symmetries, in combination with experimental visualization of vortex matter in mesoscopic samples, either via Bitter decoration, or scanning probe (STM or scanning Hall) measurements can be used to detect the presence of interaction anisotropy and consequently unconventional pairing in novel superconductors.

Usage: Lihao Yan's Senior Thesis for B.S. Physics at the University of Notre Dame.

Keywords: Anisotropic Order Parameter, Mesoscopic Superconductors, Unconventional Superconductors, Energy Landscape, Numerical Ginzburg-Landau Theory

CONTENTS

I. INTRODUCTION

A. A Brief History Of Superconductivity

Upon its first discovery in 1911 by Heike Kamerlingh Onnes, superconductors have gained enormous attention in both academia and industry. Using liquid helium, Onnes was able to cool various materials to a temperature that the electrical resistance completely disappears[1]. These type of materials are known as the superconductors ever since. Another characteristic of superconductors is their perfect diamagnetism known as the Meissner-Ochsenfeld effect, which means that the materials expel the magnetic field lines (see Fig. 1)[1, 2]. The magnetic flux is still able to penetrate the surface of the superconductors with an exponential decay and forms the so called Meissner current. The characteristic width of the Meissner current is called the penetration depth λ, which indicates how far the magnetic flux penetrates into the superconducting material.

The superconducting state of a material is often obtained under low temperature, high pressure, and weak magnetic field regime. The phase diagram for some superconductors is shown in the Fig. 2. The points where the superconducting state is destroyed are called the critical points, where the corresponding temperature is called the critical temperatures, likewise the critical fields, and the critical pressures. The critical behaviors of superconductors is one of the most heated topics because it could lead to potential real world applications[3]. Superconductors can be used as the magnets for particle colliders, the Magnetic Resonance Imaging devices. They could also reduce the energy dissipation in electrical power transmissions.

When the applied magnetic field is too strong, the Mercury superconductor that Onnes discovered exits the superconducting state suddenly as shown in Fig. 3. In 1935, Rjabinin and Shubnikov observed that for some other superconductors, as the applied magnetic field increases, the magnetic flux penetrate into the superconductors while the superconductors experience a mixture of normal state and the superconducting state before completely return to the normal state. This type of superconductors is thereafter referred to as the Type-II superconductors while the superconductors that exit superconducting state suddenly are called the Type-I superconductors. Their difference is best illustrated in the Fig. 4. The mixed state has several special properties, one of which being that the magnetic field

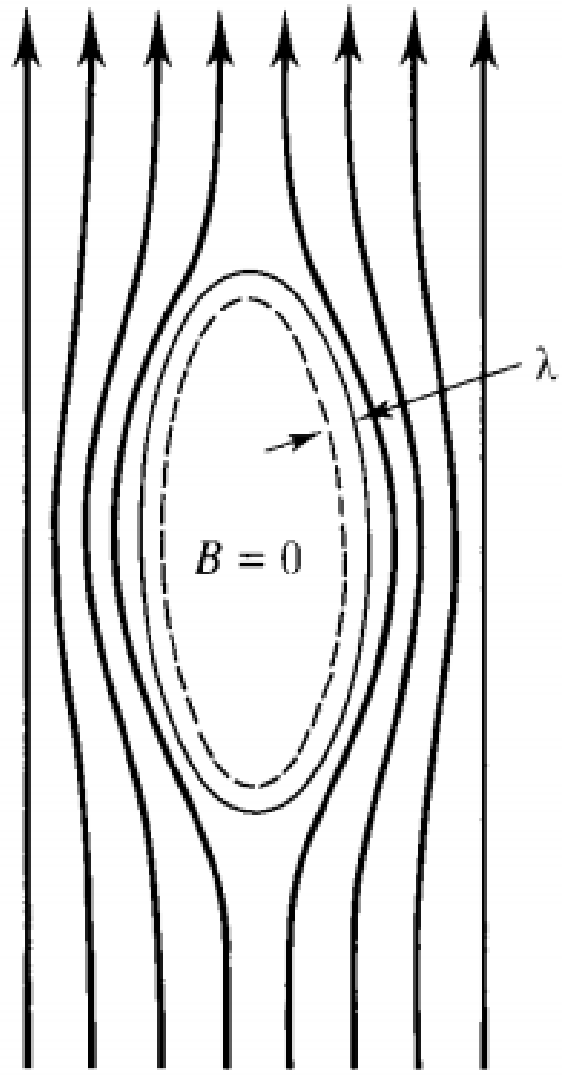

FIG. 1: Schematic showing that magnetic field lines are repelled away from the superconducting material. λ is the penetration depth.

penetrate through the superconductors in the form of vortices. The Fig. 5 shows that the Type-II superconductors are able to maintain the superconducting state at a much higher temperature, which allows them to have greater application potential.

There are two mainstream theories explaining the phenomenon of superconductivity: the microscopic Bardeen-Cooper-Schrieffer theory (BCS)[5] and the phenomenological Ginzburg-Landau (GL) theory[6]. When the GL theory was first proposed, it was believed to be a phenomenological theory. It turns out later that the BCS theory becomes the GL theory near

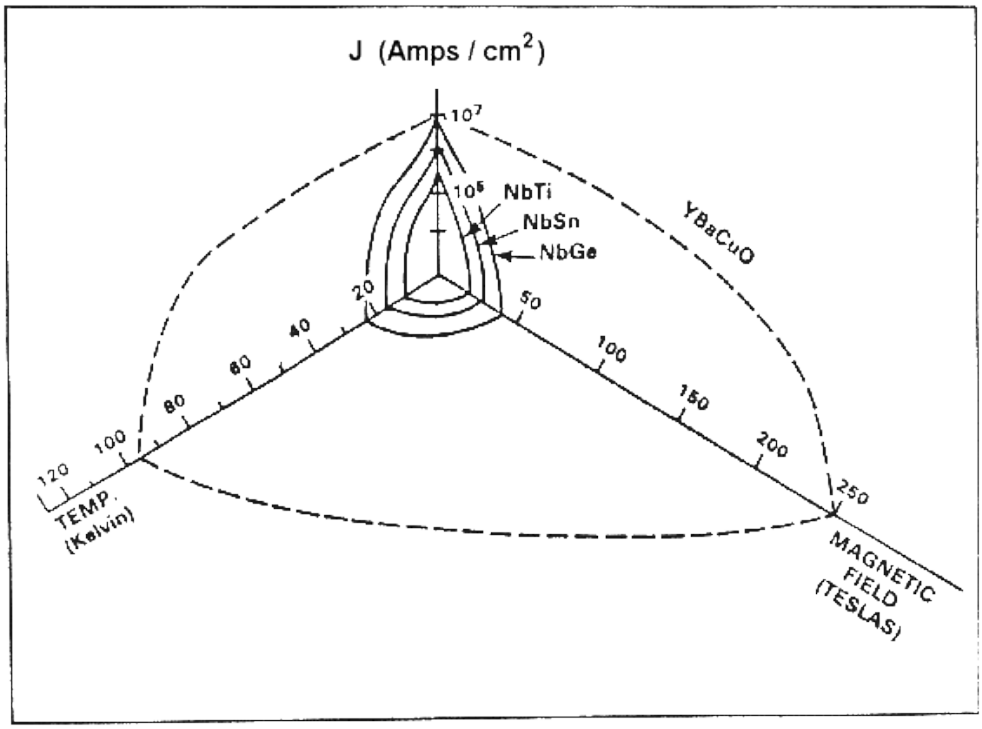

Phase Diagram

FIG. 2: Phase diagram for several different superconductors[4].

the critical temperature T_c[1, 7]. In this project, we will focus on using the Ginzburg-Landau theory to study the unconventional superconductors, where the BCS model based on electron-phonon coupling is invalid[8]. The cooper pairs in the unconventional superconductors are most likely bound by exchange other than the phonon-exchange. However, GL theory is still applicable to study the vortex structures in the unconventional superconductors.

The GL theory was first proposed by two Soviet physicists Lev Lazarevich Davidovich Landau and Vitaly Ginzburg in 1950. In the GL theory, they introduce an additional parameter called the coherence length ξ. The ratio $\kappa = \lambda/\xi$ is known as the Ginzburg-Landau parameter. A superconductor belongs to Type-I superconductors if $0 < \kappa < 1/\sqrt{2}$, and belongs to Type-II superconductors if $1/\sqrt{2} < \kappa$.

One of Landau's students, Alexei Abrikosov, further develops the GL theory for Type-II superconductors and predicts the existence of quantized magnetic flux penetrating through the Type-II superconductors in 1957[9]. In Fig. 7, Tinkham demonstrates how the vortices arrange themselves, and in Fig. 8 Bending shows what vortex tube may look like in the presence of the anisotropic interaction. These quantized magnetic fluxes are called the

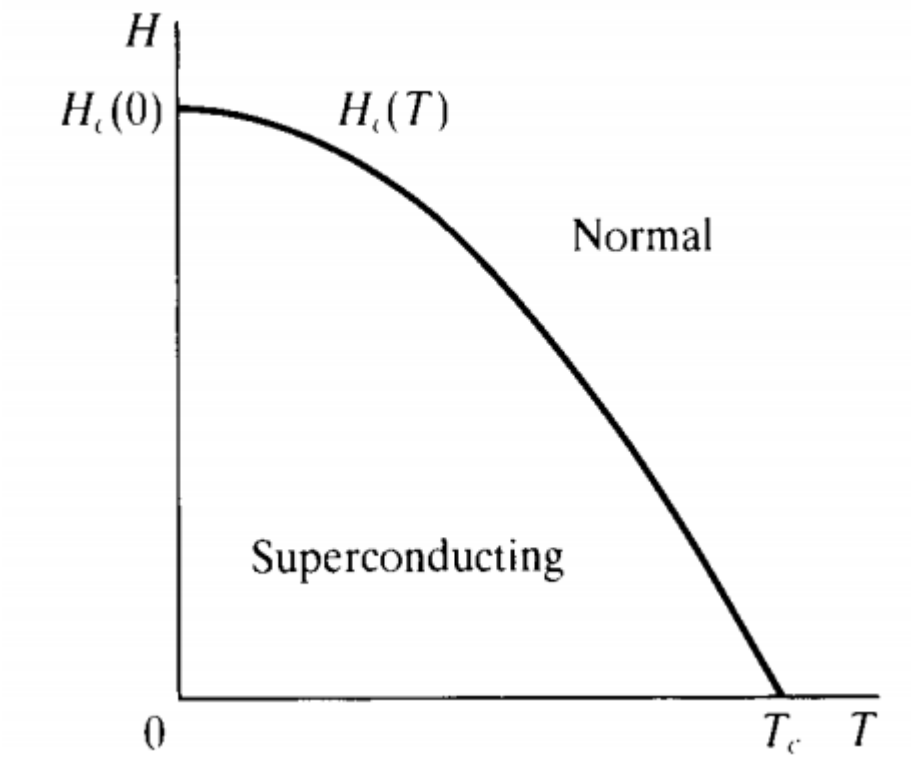

FIG. 3: Phase diagram for Type-I superconductors, where T_c stands for the critical temperature and H_c stands for the critical field.

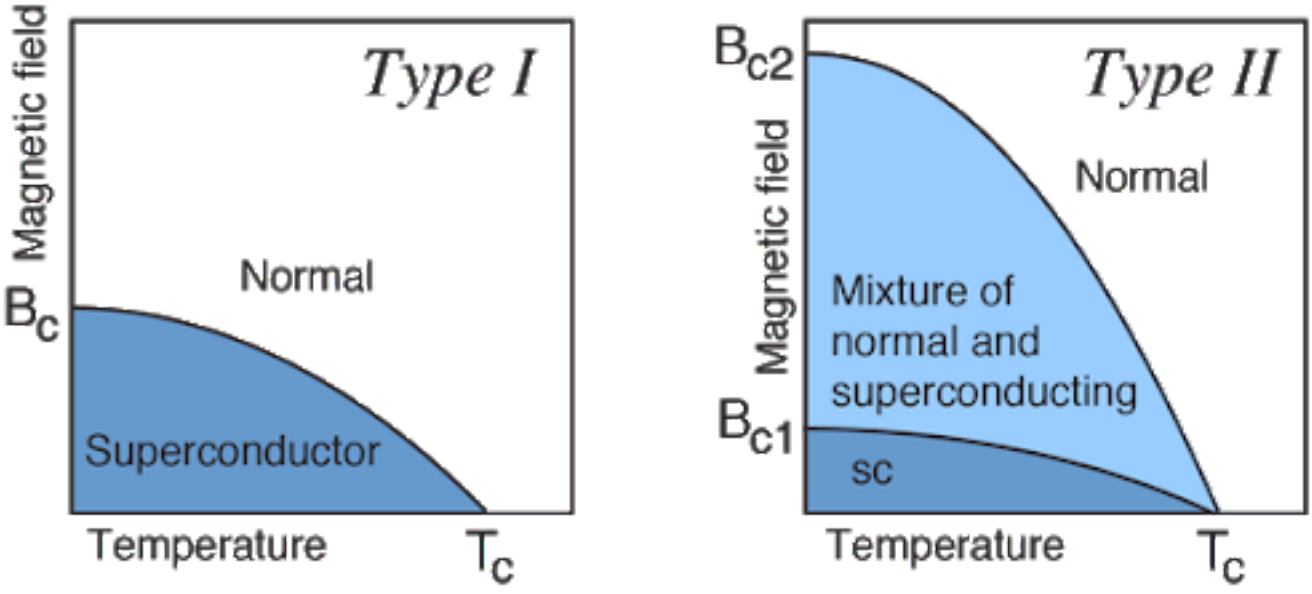

FIG. 4: Phase diagram for Type I and Type II superconductors in comparison.

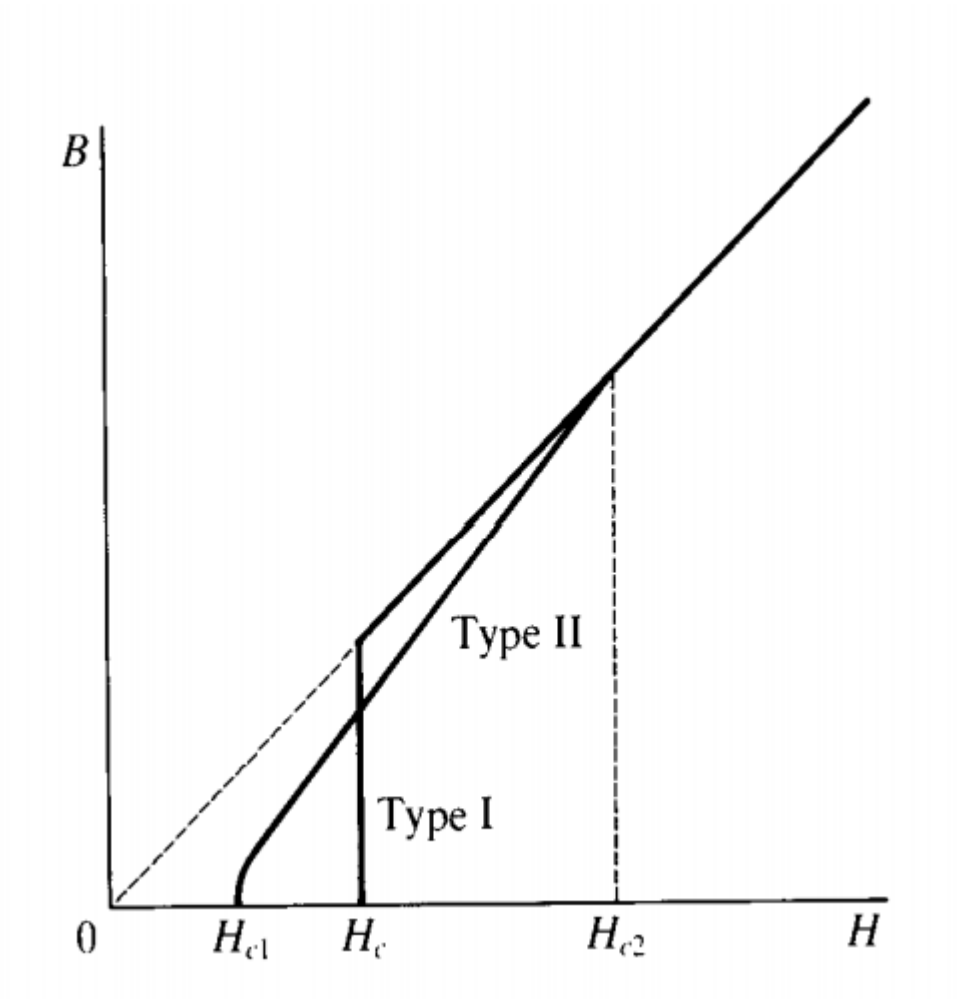

FIG. 5: Comparison of how the magnetic field penetrates through the Type-I and Type-II superconductors.

Abrikosov vortices, which were observed experimentally using small-angle neutron diffraction in 1964 and then confirmed again using the Bitter decoration technique in 1967[10, 11]. The highly plausible observation of the vortices from Essmann, et al. is shown in Fig. 6. The triangular lattice of the vortices in the bulk superconducting material can be clearly identified in the image.

The emergence of vortices is one of the unique properties of the Type-II superconductors[12]. Vortex matter soon became a heated field of research ever since. Instead of viewing the vortices as a system of rigid rods, the vortices could be considered as a system of interacting line objects. These vortices have non trivial statistical mechanics and can be seen as a new form of matter, which is known as the "vortex matter"[13]. As the vortices penetrate

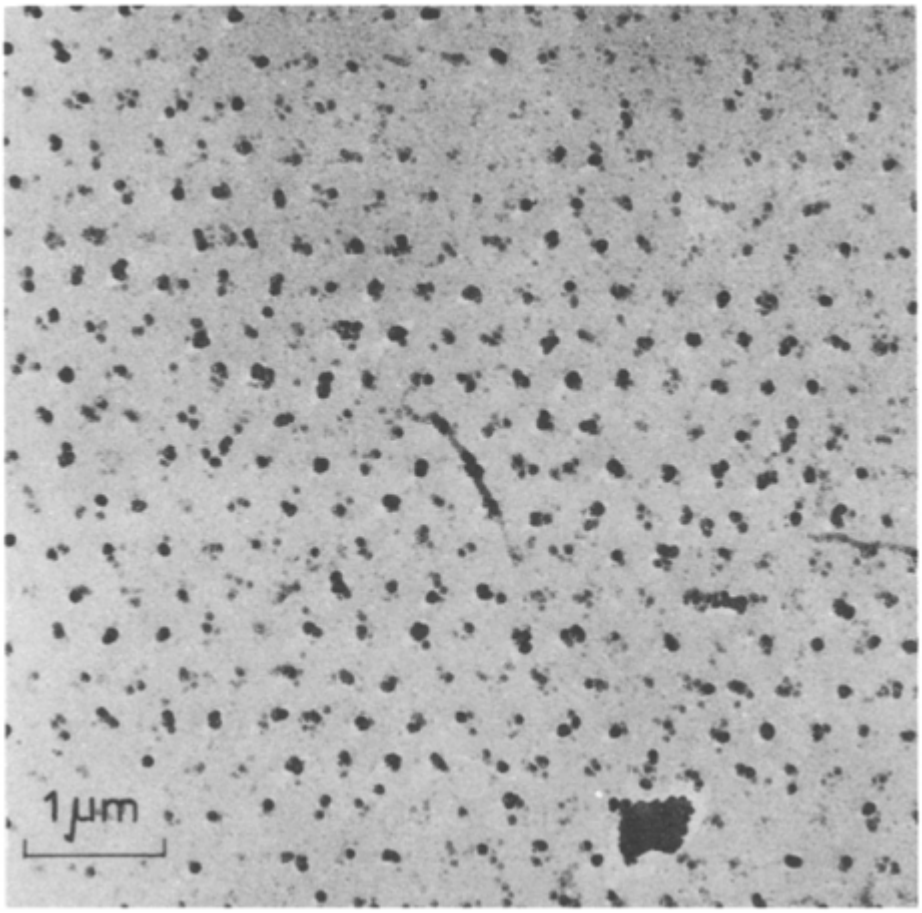

FIG. 6: Observation of vortices on the surface of a lead-4a% indium rod at 1.1^oK using the Bitter Decoration technique.

through the superconducting materials, they will move in the presence of an electrical current, dissipating energy, and causing electrical resistance. However, at the same time, their structures reflect the underlying interaction of the superconductors, which, in turn, could potentially point to unconventional pairing in an unconventional superconductor.

One important branch of the vortex matter is the study of vortex structures, which means how the vortices arrange themselves in the superconductors. The structure of the vortices reflects the different interaction within the superconductors. For example, in bulk superconductors with isotropic interaction, we have observed triangular lattices as shown in Fig. 6. In circular mesoscopic superconductors with isotropic interaction, we observe circular shell-like vortex structures as shown in Fig. 11. The underlying interaction can also lead to anisotropic order parameters, which could be used as the evidence for unconventional

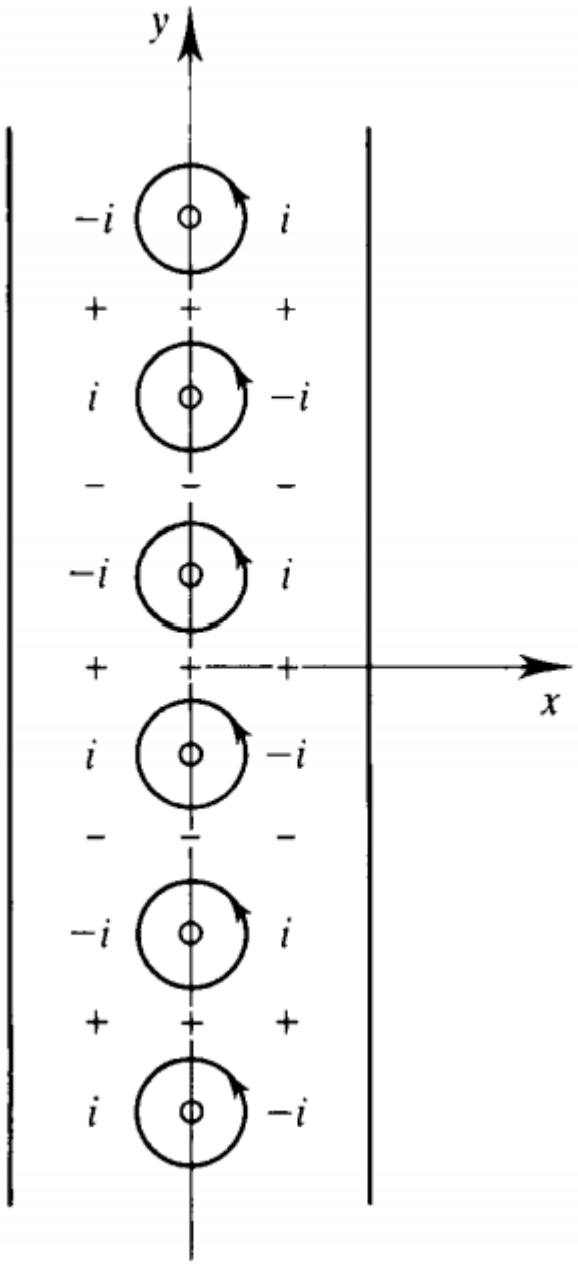

FIG. 7: Vortices in superconducting film.

superconductivity.

Unconventional superconductors have drawn much attention in the recent years following the 1979 discovery of the $CeCu_2Si_2$ superconductor by Steglich, et al.[14]. They are uncon-

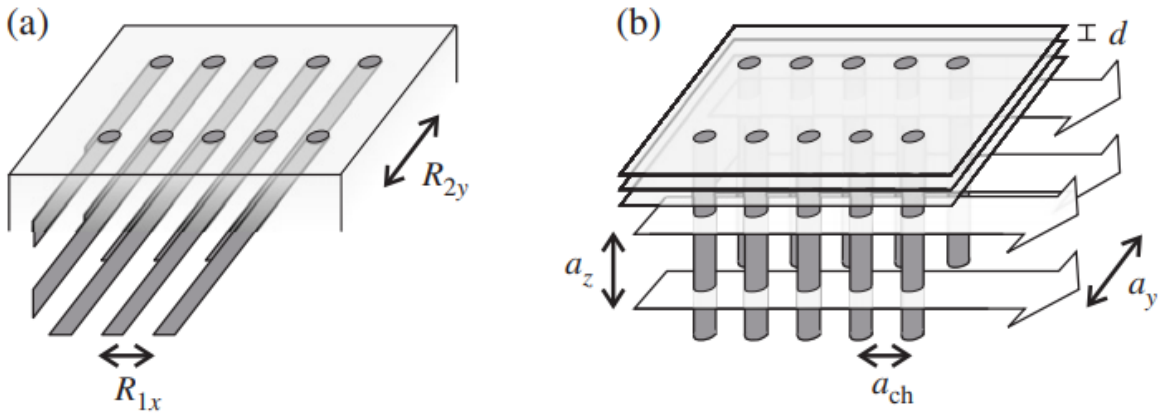

FIG. 8: Schematic for vortices in the presence anisotropic interaction.

ventional in the sense that they cannot be described by the BCS model. The unconventional superconductors attract people's attentions because sometimes they have much higher critical temperatures comparing to the traditional superconductors, which suggests that they have greater potential in device applications. Another unique property of the unconventional superconductors is that they exhibit symmetry breakings, e.g. time reversal and reflection symmetry breaking. In this project, we are interested in the reflection symmetry breaking, which implies that the unconventional superconductors have anisotropic order parameters, i.e. p-, d-, and f-wave. Nonetheless, the unconventional superconductors are notoriously difficult to identify experimentally[8]. Some experimental measures for the unconventional superconductors are magnetic resonance below the critical temperature, the existence of power law for various properties, and the existence of an anisotropic order parameter[8].

Another interesting research topic in superconductivity is the study of mesoscopic superconductors. Those superconductors often lead to counterintuitive observations like giant vortices[15] and fractional vortices[16]. They also have unusual electromagnetic properties[17]. The most important property of the mesoscopic superconductors is its confinement effect or the wall effect, where the edges of the containers exert forces on the vortices in the superconductor and affect their vortex structure. In the case of the fractional vortices, Chibotaru, et al. predicts that the confinement effect will stabilize the fractional vortices[16]. In this project, we are interested in the interplay between the anisotropic interaction between the vortices and the confinement effect. For the vortices in mesoscopic superconductors, the geometry of the superconductor determines the shape of the vortex structure. For mesoscopic

superconductors with isotropic interaction, the geometries of the vortex structures often reflect the geometry of the samples those vortices are in. The vortex structures conform with the shape of the mesoscopic container. They also form the so-called magic number states that exhibit shell like structures and higher stability for some magic number of vortices[18].

The vortex matter has also been studied greatly in experiments. Common techniques used in observing vortices includes SQUID, Bitter decoration, and STM techniques. We will give some examples of the experimental observation results using these techniques in Section I C.

B. Ginzburg-Landau Theory For Vortex Matter

In this section, I will give a concise summary of the Ginzburg-Landau theory for vortices[1]. GL theory introduces a macroscopic function ψ that describes the superconducting electrons, where the local density of superconducting electrons are defined as

$$n_s = |\psi(x)|^2. \tag{1}$$

The idea is to expand the free energy in a series with coefficients α and β and use variational principle to obtain the GL differential equation:

$$\frac{1}{2m^*}(\frac{h}{i}\nabla - \frac{e^*}{c}A)^2\psi + \beta|\psi|^2\psi = -\alpha(T)\psi. \tag{2}$$

I now define the penetration depth and the coherence length and introduce the famous GL parameter. The penetration depth λ and the coherence length ξ are defined as

$$\lambda(T) = \frac{\lambda(0)}{|1-(T/T_c)^4|^{1/2}}, \tag{3}$$

and

$$\xi(T) = \frac{\hbar}{|2m^*\alpha(T)|^{1/2}}. \tag{4}$$

The GL parameter is defined as

$$\kappa = \frac{\lambda}{\xi}, \tag{5}$$

which is a constant approximately independent of temperature. One important implication of the GL parameter, shown by Abrikosov, is that $\kappa = \sqrt{2}$ is the critical value of distinguishing between Type-I and Type-II superconductors.

In 1957, Abrikosov showed the existence of flux tubes between the H_{c1} and H_{c2}, which is the mix state region shown in Fig. 4 and Fig. 5. In the mix state, the magnetic field starts

to penetrate into the superconductor before the superconductivity is completely destroyed. Each vortex carries a quantum of flux

$$\Phi_0 = \frac{hc}{2e}. \tag{6}$$

The vortices can move around in the superconductors driving by external forces or thermal fluctuations. Another property of vortices is that they experience repulsive forces between each other. In the approximation $\kappa >> 1$, the interaction force between the vortices is

$$F_{12} = \frac{\Phi_0^2}{8\pi^2\lambda^2} K_0(\frac{r_{12}}{\lambda}). \tag{7}$$

This repulsive force will be very useful in our energy landscape calculation.

C. Experimental Investigations Of Vortex Matter

Since its first discovery, vortex matter has been studied both experimentally and theoretically. I have described the theoretical basis for the vortex matter in Section I B, and now I would like to describe the experimental observations of vortex matter in various superconductors. Some common techniques used to investigate the vortex structures are scanning electron microscopy (SEM)[19], scanning tunneling microscopy (STM)[15, 20, 21] scanning hall probe microscopy (SHPM)[22], Bitter decoration[11, 23], and scanning superconducting quantum interference device microscopy (SQUID)[7, 24]. Sometimes these techniques are used in combination.

For the bulk superconductors, I have already mentioned the famous observation by Essmann using the Bitter decoration (see Fig. 6). The lead-indium superconductor Essmann observed belongs to the conventional Type-II superconductors. In this project, we will focus on the experimental observations of mesoscopic superconducting samples and unconventional superconductors. We will present experimental observations of both the mesoscopic superconductors and the unconventional superconductors. The experimental examples below show that the experimental configuration we are proposing in this project is viable and will also serve as a justification for the simulation results in the later sections.

1. *Mesoscopic Superconducting Samples*

Experimentalists could pattern superconducting samples via e-beam and focused ion beam lithography into different mesoscopic shapes and apply different magnetic fields onto the sample. According to equation (6), each vortex carries a fixed number of magnetic flux. Therefore, the strength of the magnetic field determines the number of vortices in the mesoscopic container. In this section, we show the experimental results for triangular samples, square samples, and circular samples under different magnetic fields. The experimental observations mentioned in this section are observations of conventional superconductors with isotropic vortex-vortex interaction.

The vortices in triangular samples are shown in Fig. 9. This experiment was done by Zhao, et al. using SEM and Bitter decoration[25]. The observed results qualitatively agrees with our simulation results in Fig. 20.

Zhao's group also investigated the square samples[26], where again they have used SEM and Bitter decoration. The experimental results are shown in Fig. 10.

In 2006, Grigorieva's group studied the circular samples using SEM and bitter decoration[18] the results are shown in Fig. 11.

2. *Unconventional Superconductors*

As mentioned above, the unconventional superconductors often have anisotropic interaction between the vortices as a result of their anisotropic order parameters. Consequently, we seek to predict anisotropic order parameters by identifying the anisotropic interaction between the vortices.

One of the strongest evidences for the existence of the anisotropic interaction in $Bi_2Sr_2CaCu_2O_{8+\delta}$ (BSCCO) is the observation of the vortex chian states in BSCCO shown in Fig. 12. This observation qualitatively agrees with our simulation results shown in Fig. 18 and the numerical Ginzburg-Landau calculations.

Another example for unconventional superconductor is the Pb island growing on the undoped Si(111)[15, 27, 28] that is shown in Fig. 13.

MgB_2 is an unconventional superconductor that has measured anisotropy γ_x, which is the ratio between the of perpendicular directions[19, 29]. The SEM imaging of the vortices in

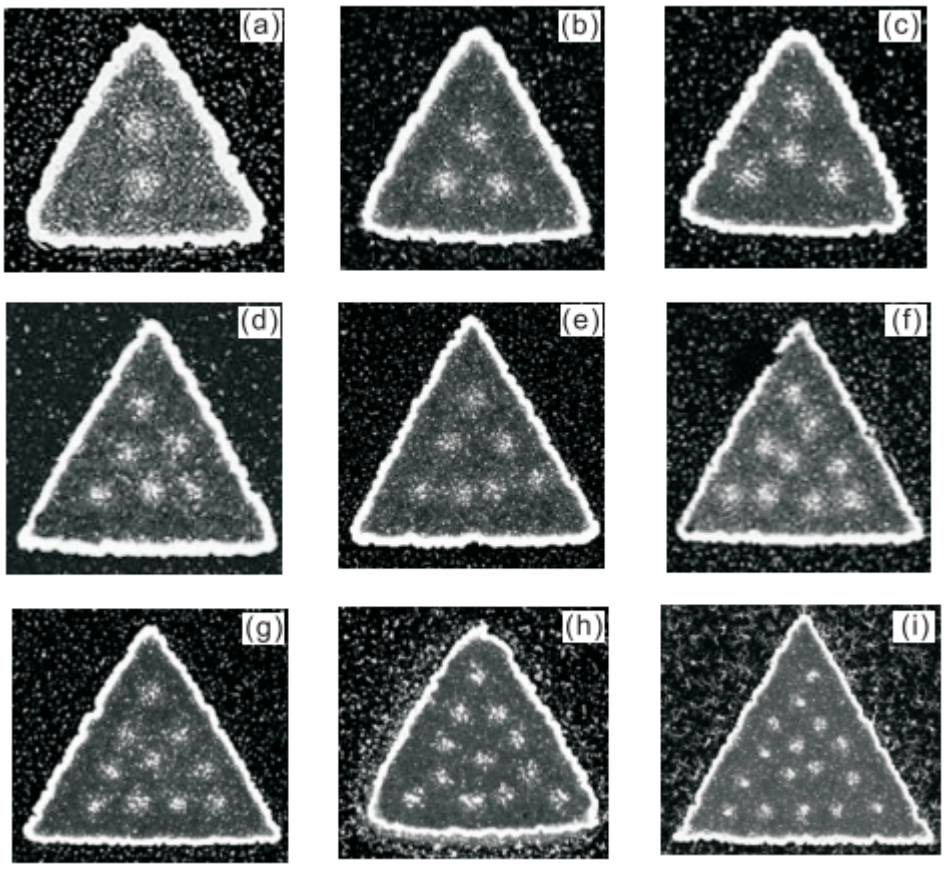

FIG. 9: SEM images of vortices in triangular samples made of thick Nb film deposited on a Si substrate using magnetron sputtering. The number of vortices ranging from 2 to 16 in the samples.

single MgB_2 crystal at low magnetic field is shown in Fig. 14. The γ_x for MgB_2 is estimated to be approximately equal to 2.5.

The last unconventional superconductor I want to show here is the $Y_1Ba_2Cu_4O_8$ (YBCO-124)[7, 30]. An vortex structure imaging obtained using Bitter decoration is shown in Fig. 15 The anisotropy in a-b plane is measured to be approximately equal to 1.4, where the a-b plane is defined in Fig. 8 and the anisotropy is just the relative ratio of the interaction strength in the perpendicular direction. I will use the anisotropy of the YBCO-124 as the weak anisotropy limit in our rescaling theory calculation.

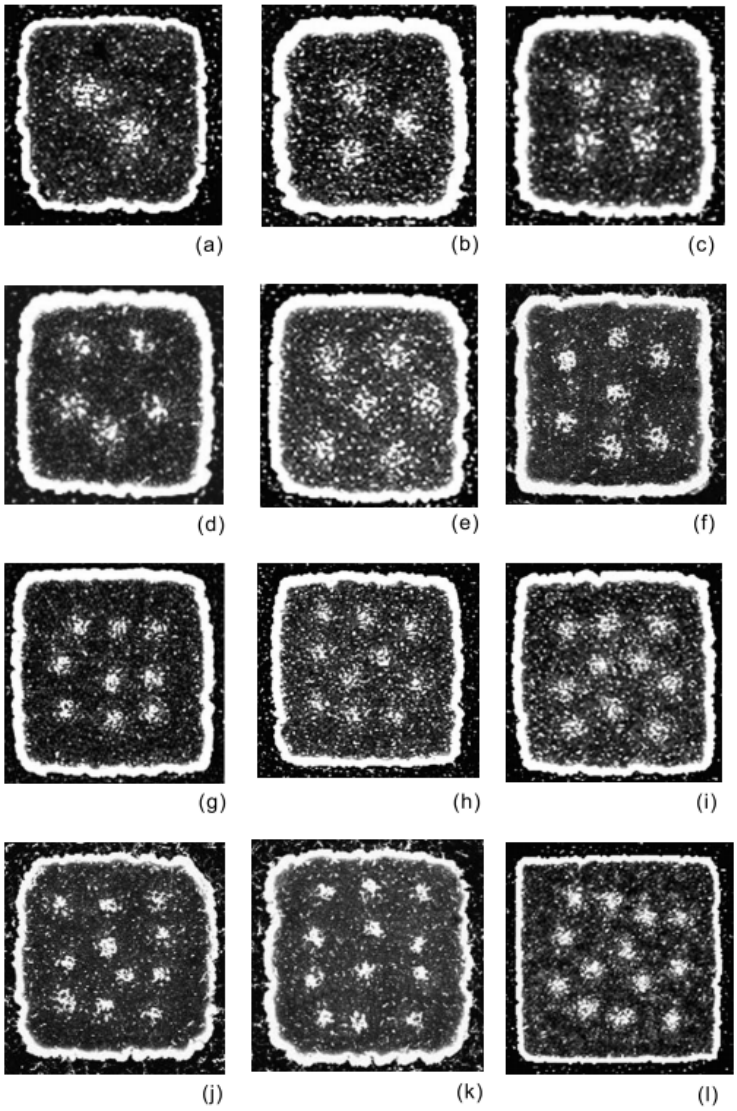

FIG. 10: SEM images of vortices in triangular samples made of thick Nb film deposited on a Si substrate using magnetron sputtering. The number of vortices ranging from 2 to 13 in the samples.

II. OVERVIEW AND MAIN RESULTS

One of the main challenges in the field of superconductor is the identification of novel unconventional superconductors. One of the key properties of the unconventional superconductors is the existence of anisotropic order parameters, which leads to the anisotropic interaction between the vortices in the superconductors. While the anisotropic interaction is hard to identify on its own, we argue that the interplay between the anisotropic interaction

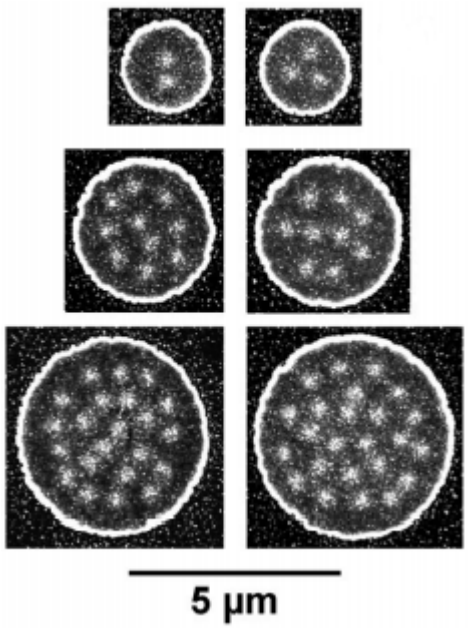

FIG. 11: SEM images of vortices in triangular samples made of thick Nb film deposited on a Si substrate using magnetron sputtering. The disks are $d = 2.3, 3.4,$ and $5.0\mu m$ in diameter respectively.

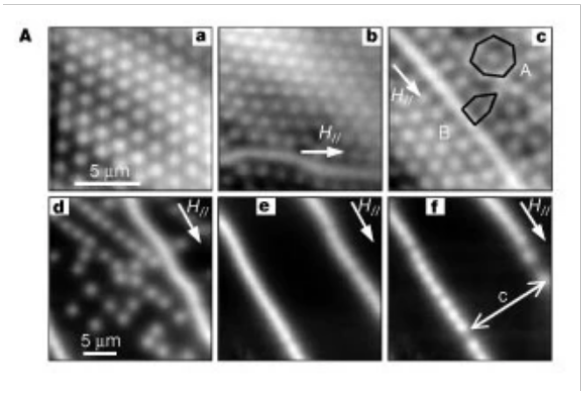

FIG. 12: SHPM images of vortex chain in the BSCCO in the strong anisotropy regime.

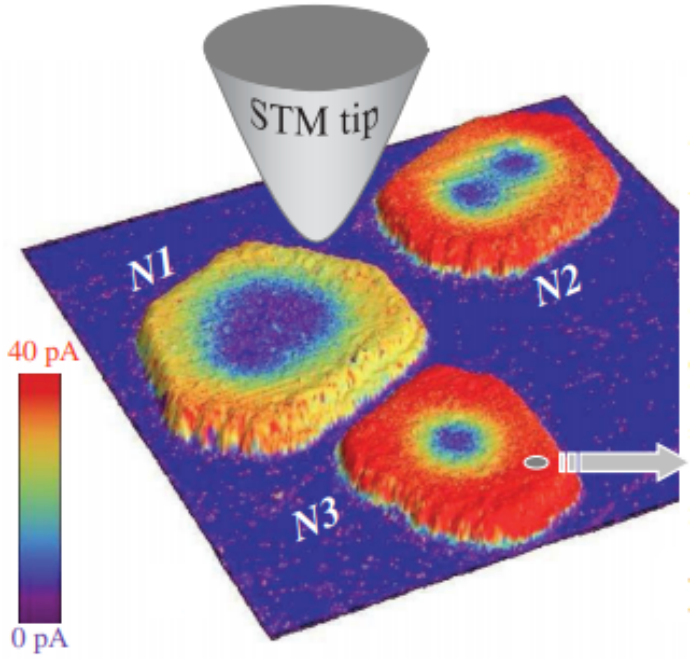

FIG. 13: STM images for the vortices in the Pb island. The smallest island N3 has one vortex and the middle size island N2 has two vortices, so the largest island N1 should have three vortices instead of one giant vortices. This is probably due to the confinement effect of the Pb island [15].

and the confinement effect due to the container wall will amplify the effects of anisotropy at certain magnetic field. With a smart combination of the container shape and magnetic field, we could devise experiments that the anisotropic interaction in the superconductors become the most evident.

In this work, we investigate both the weak and strong anisotropy regime. In the weak anisotropy regime, we seek to identify the interaction using the special wall effect of the mesoscopic superconductors by making a optimized choice of the container geometry. We solve for the energy landscape of the mesoscopic samples to find the ground state vortex configurations of different vortex numbers and different container shapes. We compare the configurations to find the container geometry that is best at identifying the anisotropic interaction between the vortices. We show that the vortex structure of eight vortices in triangular samples has a qualitative difference in the presence of weak anisotropic interaction. We conclude that the containers with low symmetry, e.g. triangular containers, are best at

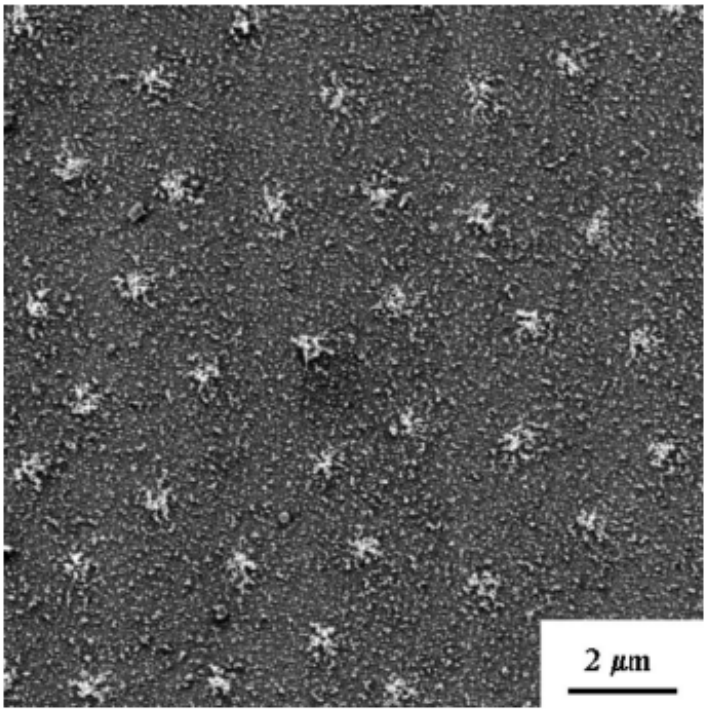

FIG. 14: MgB_2 sample that does not form a regular triangular lattice due to its underlying anisotropic interaction.

identifying the anisotropic interaction between the vortices.

In the strong anisotropy regime, we observe the formation of vortex chains in the superconductors, which could also be used as evidence for the existence of anisotropic interaction. In the later part of our project, we seek to verify our calculation using the numerical Ginzburg-Landau theory proposed by Milošević and Geurts[31]. We have qualitatively confirmed the emergence of the vortex chains in superconductors for the strong anisotropy regime. We will verify our calculation for the weak anisotropy regime in the future.

III. ENERGY LANDSCAPE CALCULATION

In order to find the best container geometry that can be used to identify experimentally the anisotropic interaction between the vortices, we survey different container geometries to find geometry that the anisotropic interaction is the most evident from its vortex structures.

We calculate the ground state vortex structures by solving the potential energy landscape of the system. There are two main contributions to the potential energy of the system:

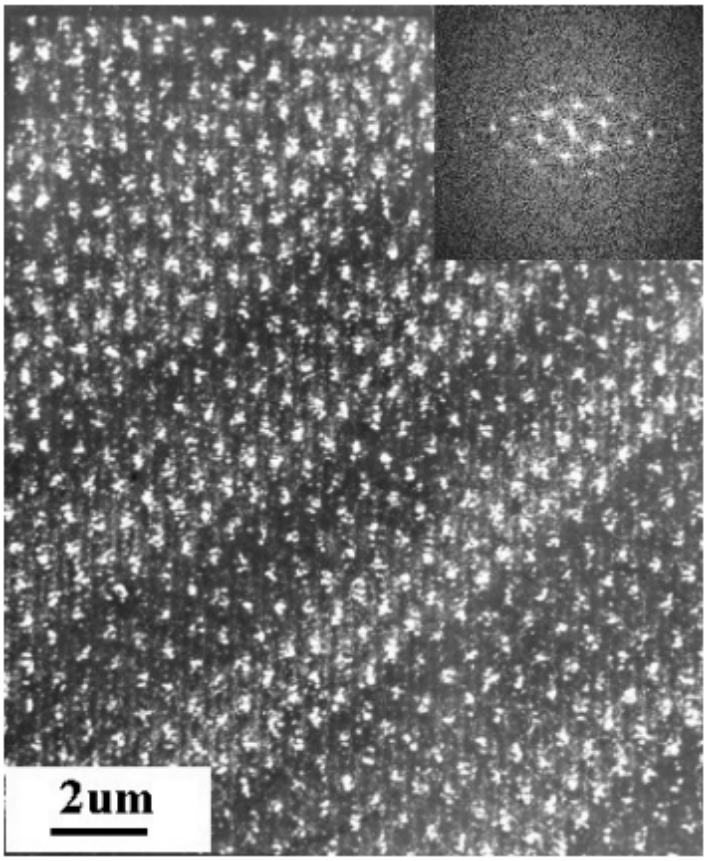

FIG. 15: Vortices in YBCO-124 sample with a Fourier transform of the image at the top right-hand corner.

the vortex-vortex interaction and the confinement effect from the sample. The strength of both interaction depend on the locations of the vortices, so we can define a potential energy landscape as a function of the locations of the vortices. The locations of the vortices at the minimum potential energy will be the ground state vortex structure configuration. Using the energy landscape, we are able to produce theoretical results that are in qualitative agreements with the experimental observations described in Section I C.

Since the Abrikosov vortices in the superconductors have translational symmetry in the direction parallel to the external magnetic field[1, 7], we can treat the Abrikosov vortices as 2D quasiclassical particles lying in the same plane that is perpendicular to the direction of the magnetic field. The location $\vec{r} = (x, y)$ of each vortex is defined by the coordinate of its center. For a system of n vortices the potential energy landscape of the system is a function

of $2n$ dimensions:

$$E_{total}(\vec{r}_1(x_1, y_1), \vec{r}_2(x_2, y_2), ...) = \sum_{i,j} E_{vv}(\vec{r}_i, \vec{r}_j) + \sum_i E_{wall}(\vec{r}_i), \tag{8}$$

where E_{vv} is the vortex-vortex interaction energy and E_{wall} is the energy of the vortices due to the walls of container.

In Type-II superconductors, the vortices experience a repulsive force between each other[1] and with the container walls. For isotropic interaction between the vortices, the vortex-vortex interaction assumes the form of a modified Bessel function in equation (7). In our simulation, we simplify the equation (7) to the following equation:

$$E_{vv}(\vec{r_i}, \vec{r_j}) \propto K_1(r), \tag{9}$$

where $r = |\vec{r_i} - \vec{r_j}|$ and K_1 is the modified Bessel function of first or zeroth order. λ is the penetration depth, which is chosen to be unity in the isotropic calculation. We are allowed to omit factors in front of the Bessel function because the overall factors in front of the Bessel function in equation (7) does not affect much the structure of the vortex configurations, which is what we are primarily concerned with.

To characterize the confinement of the container, we assume a simple $1/r$ repulsive forces between each vortex and the container walls. For circular container, the potential energy assumes the following form:

$$E_{wall}(\vec{r_i}) \propto \frac{|\vec{r_i}|}{(a - |\vec{r_i}|)^2}, \tag{10}$$

where a is the radius of the circular container. Since we assume that the container is centered at $(0, 0)$, the term $a - |\vec{r_i}|$ is the shortest distance of the vortices to the edges of the circular container. For other container geometries, the potential energy depends on the distance from the center of the vortices to each side of the container:

$$E_{wall}(\vec{r_i}) \propto \sum_w \frac{1}{r_{wi}}, \tag{11}$$

where r_{wi} is the distance from the center of the vortices to the wall and we sum over all the sides of the container. In our calculation, we will set all the proportional factors to unit. The energy landscape defined above is shown in Fig. 16.

In the rest of this section, we survey different configurations by solving for the ground state of the energy landscape of both the isotropic interaction and anisotropic interaction using

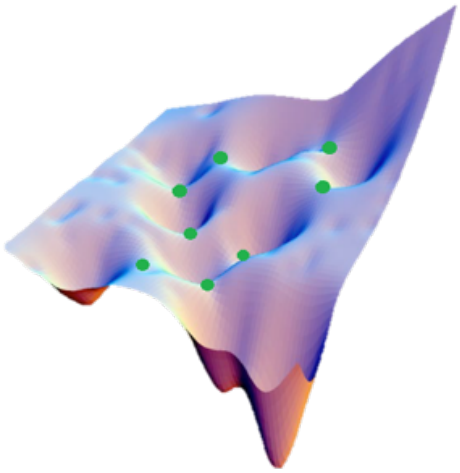

FIG. 16: Energy landscape defined in equation (8) with isotropic vortex-vortex interaction. The green points indicate the transition states between the ground states.

the eigenvector following method. We will use two different ways to simulate anisotropic interaction between vortices and discuss the calculation results of both of them. We use a phenomenological equation to study the anisotropy between the vortices. We also use the rescaling theory. We are able to use the phenomenological equation to reproduce the vortex chain states observed in BSCCO in Fig. 12. For the rescaling theory, we argue that the mesoscopic samples with low symmetry is best at identifying the anisotropic interaction in the superconductors.

A. Eigenvector Following Method

To solve for the ground state configuration of the energy landscape, we use the eigenvector following method, which is a common method in the energy landscape search[32, 33]. The eigenvector following method is a upgraded version of the Newton-Raphson method[34]. It gives a simple modification to Newton-Raphson's search step[35]

$$\mathbf{h} = \sum_i \frac{-F_i}{(b_i - \lambda)} \mathbf{u_i}, \tag{12}$$

where λ can be interpreted as a shift parameter on the Hessian eigenvalue b_i. The eigenvector following algorithm utilizes the rational function approach and gives the following two equations of λ[36, 37],

$$(\mathbf{H} - \lambda)\mathbf{h} + g = 0, \tag{13}$$

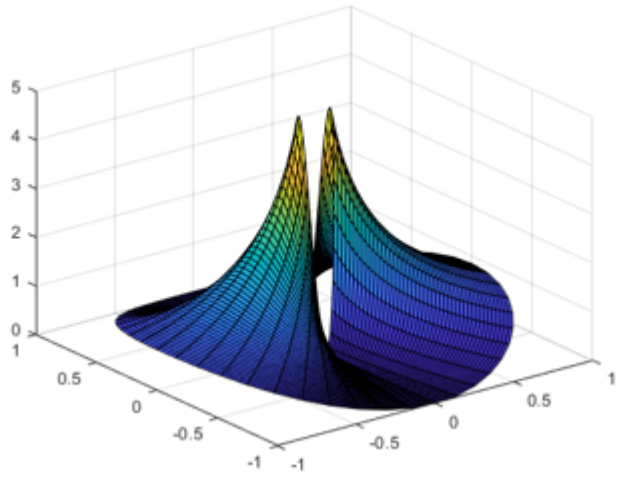

FIG. 17: Anisotropic interaction potential energy between two vortices.

and

$$\mathbf{g}^T\mathbf{h} = \lambda, \tag{14}$$

where $\mathbf{H}$ is the function of interest and g is the gradient of the function at a specific point. Solving the above two equations gives the self-consistent equation

$$\sum_i \frac{-F_i^2}{(b_i - \lambda)} = \lambda, \tag{15}$$

which can be used to solve for λ recursively.

The benefits of using the eigenvector-following method is that it has increased stability comparing to the Newton-Raphson method. In computational chemistry, the eigenvector-following method can be used to find the transition state[32, 33]. In this project, we only use the eigenvector following to solve for the ground state energy of the system.

B. Phenomenological Equation

1. Phenomenological equation

As pointed out above, the vortex-vortex interaction takes the form of a modified Bessel function defined in equation (9). Therefore, we could assume the anisotropic vortex-vortex interaction has similar forms but with different interaction strength in different directions.

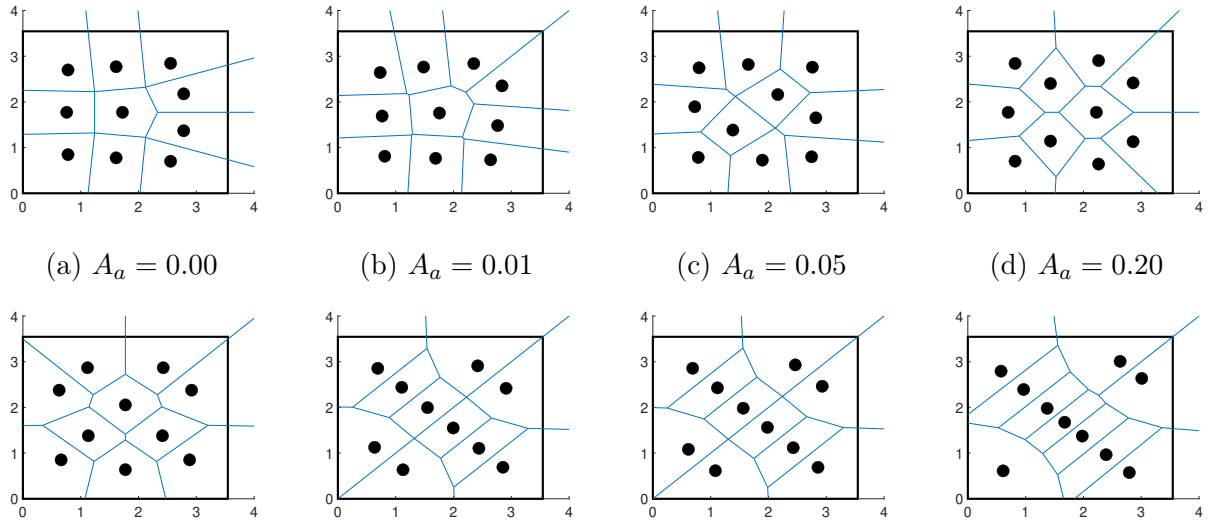

(a) $A_a = 0.00$ (b) $A_a = 0.01$ (c) $A_a = 0.05$ (d) $A_a = 0.20$

(e) $A_a = 0.50$ (f) $A_a = 0.70$ (g) $A_a = 1.00$ (h) $A_a = 3.00$

FIG. 18: Stable configurations for ten vortices in a square container under different anisotropy.

This is the approach Olszewski, et al.[38] took in their phenomenological anisotropic equation

$$E(r,\theta)_{vv} = A_v K_0(r)[1 + A_a \cos^2(\frac{n_a(\theta)}{2})], \tag{16}$$

where $r = |\vec{r_i} - \vec{r_j}|$ as usual , A_v is the overall interaction strength, A_a is the strength of the anisotropy, n_a is the number of strong interaction axes, and $\theta = \tan^{-1}(r_y/r_x)$ is the angle between the two vortices with respect to the positive axis. The anisotropic interaction energy between two vortices is demonstrated in Fig. 17.

2. Calculation Results

In our calculation, we take $A_v = 1$ because it is an overall strength factor that does not affect the vortex structure much. We take $n_a = 4$ because four-fold anisotropy is very common in unconventional superconductors. For example, the YBCO-124 has four-fold anisotropy in a specific plane[7]. We simulate the system of ten vortices because ten is enough to observe the vortex structure and it is not too many where the confinement effect is no longer significant. The A_a parameter controls the strength of the anisotropic interaction, which is the parameter that we will vary in this simulation.

One of the notable phenomena of the anisotropic interaction is the formation of vortex

chains shown in Fig. 12. If we observe vortex chains in our superconducting sample, we can conclude that there are underlying anisotropic interaction in the material.

In this calculation we gradually increasing A_a from 0 to 3, and solve for the stable configurations at each anisotropy strength to monitor how the vortex structure changes as a function of the anisotropy. We observe the formation of the vortex chains when we gradually increase the anisotropic interaction between the particles. The results are summarized in the Fig. 18, where we have solved for the stable configurations of ten vortices in a square container. As the anisotropy increases, the vortices start to line up in one direction and gets far away from each other in another direction. A vortex chain becomes visible when the anisotropy is larger than $A_a = 0.70$.

Before we proceed, there are several things we need to pay special attention to. We note that the stable configurations calculated from equation (16) may not accurately reflect the actual observations in the experiment. For example, in the high anisotropy limit, the vortices may get too close to each other and form the so called giant vortices[15]. However, the discussion of the giant vortice is beyond the scope of this project. Another limitation of using the phenomenological equation is that we do not know the experimental values for the parameters we used. While our calculation results agree qualitatively with the experimental observations, we do not know what materials have $A_a = 0.70$. Therefore, we develop an alternative method using the rescaling theory, which can be verified easier.

C. Rescaling Theory Approach

1. Rescaling Theory

As an alternative to the phenomenological equation, we could also simulate anisotropic interaction from the isotropic interaction using the rescaling theory[7, 39]. The rescaling theory starts from the London model that writes the supercurrent in terms of the vector potential and the phase:

$$\mathbf{j} = -\frac{c}{4\pi\lambda^2}(\mathbf{A} + \frac{\Phi_0}{2\pi}\nabla_i\phi). \tag{17}$$

This is an isotropic equation and can be generalized to study the anisotropic superconductors by taking an anisotropic penetration depth λ. We set λ_i to be different along the different

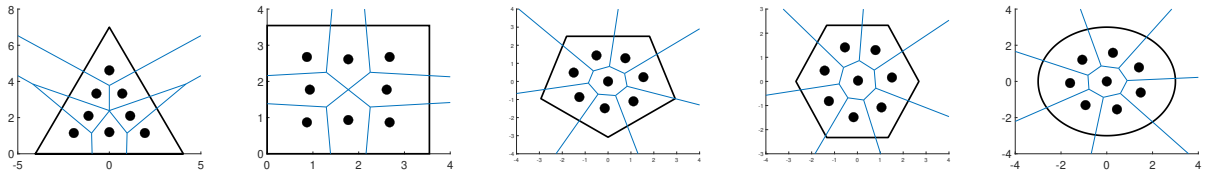

(a) samples with isotropic interaction, $\gamma_x = 1.0$

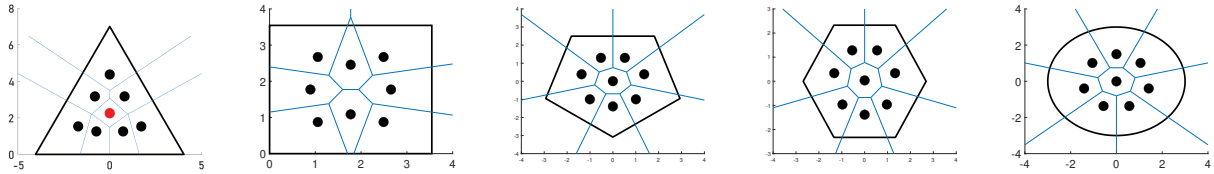

(b) samples with anisotropic interaction, $\gamma_x = 1.4$

FIG. 19: Eight vortices in different shapes of the container.

symmetry axes, so that the equation (17) becomes

$$j_i = -\frac{c}{4\pi\lambda_i^2}(A_i + \frac{\Phi_0}{2\pi}\nabla_i\phi). \tag{18}$$

We define γ_x as the ratio between the penetration depth along the two symmetry axes

$$\gamma_x = \frac{\lambda_x}{\lambda_y}, \tag{19}$$

where we set the symmetry axes to match the x-axis and y-axis in the coordinate system.

One benefit of this theory is that the ratio γ_x is a measurable quantity[19, 29] so that we can compare our simulation result with the experimental observation in actual materials. We simulate the anisotropy by rescaling the penetration depth λ_x of the x direction by the ratio γ_x. Since we set penetration depth as the unit of length in our system, multiplying λ_x with γ_x is equivalent to redefine the displacement between two vortices

$$\vec{r_{12}} = (x_2 - x_1, y2 - y1) \mapsto \vec{r_{12}} = (\gamma_x(x_2 - x_1), y2 - y1). \tag{20}$$

We then obtain the anisotropic energy landscape by plugging equation (20) into the isotropic energy landscape function defined in equation (8).

2. Numerical Results

In order to develop an experimentally viable method of identifying low anisotropy within superconducting materials, we focus on relatively low anisotropic materials like YBCO-124.

According to Bending and Dodgson[7], YBCO-124 has an anisotropy with $\gamma_x = 1.4 \pm 0.5$ in the a-b plane as defined in the Fig. 8. We surveyed different container shapes with different vortex numbers and find that the difference between the isotropic interaction and the anisotropic interaction is most evident in a triangular container with 8 vortices. Once we identify the anisotropic interaction between the vortices, we can use it as evidence for anisotropic order parameter, which possibly hint at the existence of novel unconventional superconductors.

In the simulation we set the anisotropy $\gamma_x = 1.4$ and vary the number of vortices n and the shape of the container. In actual experiments the number of vortices is related to the strength of the magnetic field. They are roughly correlated by the magnetic flux each vortex carries as shown in equation (6). The experimentalist can also sample with different shapes. In our simulation, the number of vortices determines the dimension of the potential energy (8), and the shape of the container determines the the energy of the vortex interaction with the wall E_{wall}. Since we are looking for the best sample shape, we first survey containers of different shapes with a fixed vortex number. In Fig. 19, we fix the number of the vortices to eight and survey different container shapes. We choose a relatively low number vortices because we are interested in the regime where the confinement effect plays a significant role. In the limit of many vortices, the confinement effects are weaker compared to the vortex-vortex interaction. The vortices at the center start to form triangular lattices like in the bulk materials. The choice of eight vortices will be evident shortly.

In Fig. 19 we only observe qualitative changes in triangular samples. The vortices form two shells in the presence of the anisotropic interaction but only one shell of the vortices in the absence of it. Other sample shapes don't show this kind of qualitative change. Therefore, we conclude that the triangular container works best for detecting anisotropy when there are eight vortices. We now proceed to show why we choose the container with eight vortices.

We survey different numbers of vortices in a triangular container. The results are shown in Fig. 20 and Fig. 21, We found that the presence of the anisotropic interaction is most evident when there are eight vortices in the container. We observe an extra shell of vortices in Fig. 21(c) comparing to its isotropic counterpart Fig. 20(c). We do not observe such qualitative change for other vortex numbers. This is reasonable because eight vortices is at the boundary of forming a new shell of vortices. We observe two shells of vortices in Fig. 20(d), but only one shell of vortices in Fig. 20(b). As the result of the anisotropic

interaction, the system forms another shell of vortices to minimize the total energy. The qualitative difference between the two configurations could be used to identify anisotropic interaction in the actual experiments.

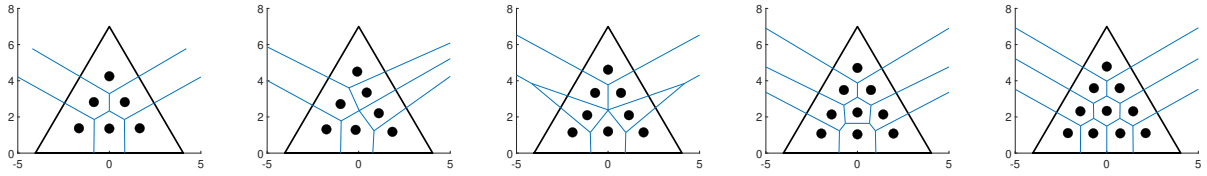

(a) $n = 6$ (b) $n = 7$ (c) $n = 8$ (d) $n = 9$ (e) $n = 10$

FIG. 20: Triangular samples with isotropic interaction, $\gamma_x = 1.0$.

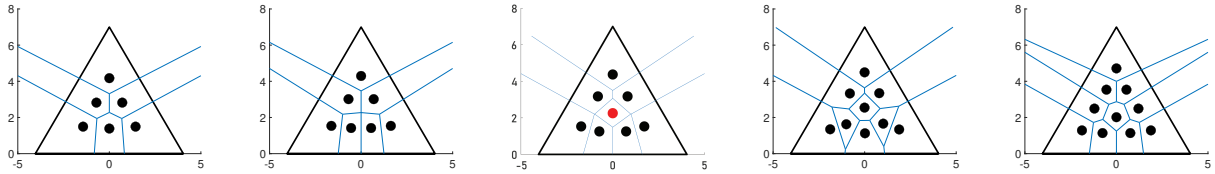

(a) $n = 6$ (b) $n = 7$ (c) $n = 8$ (d) $n = 9$ (e) $n = 10$

FIG. 21: Triangular samples with anisotropic interaction, $\gamma_x = 1.4$.

We chose eight vortices in a triangular container because that's the best configuration we found after surveying many other combinations of container shape and vortex number, which we will not have time and space to list all of them in this thesis. The Fig. 20 and Fig. 21 both show isotropic and anisotropic interaction for different vortex numbers within the low vortex regime. The underlying anisotropic interaction is most evident when there are eight vortices in the container.

One caveat worth mentioning is that in addition to the ground state configuration, there often exists other low lying stable configurations that may be observed experimentally. Nonetheless, this is a common issue people are facing in vortex observation. The vortex structure could be influenced by the impurities, temperature, and etc. Providing a solution to this problem is beyond the scope of this thesis.

IV. NUMERICAL GINZBURG-LANDAU CALCULATION

As mentioned above, the phenomenological GL equations could be adjusted to study the unconventional superconductors. The GL equations are also very useful in studying

the mesoscopic superconducting samples[40]. In 2010, Milošević and Geurts proposed a numerical approach for solving the GL theory in the mesoscopic systems that is readily applicable to simulate the actual experiments[31]. One experiment they have studied is the Pb island shown in Fig. 13. Milošević and Geurts developed their code in FORTRAN. In this project, we adopt Milošević and Geurts' FORTRAN package and adjust it to accommodate for the anisotropic interaction. We verify the formation of the vortex chains done by the phenomenological equation calculation using the numerical Ginzburg-Landau package and we are planning on to use the package to verify the rescaling theory in the future.

A. Numerical Ginzburg-Landau Theory

The numerical Ginzburg-Landau theory (NGL) has been discussed in great detail in Milošević and Geurts' paper[31]. The starting point of NGL is the free energy functional $\mathcal{F}$ with respect to ψ and $\vec{A}$

$$\mathcal{F}\{\psi, \vec{A}\} = \frac{H_c^2}{4\pi} \int \left[-|\psi|^2 + \frac{1}{2}|\psi|^4 + \frac{1}{2}|(-i\nabla - \vec{A}\psi|^2 + \kappa^2(\vec{h} - \vec{H}_0)^2 \right] dV, \tag{21}$$

where $\lambda, \xi,$ and κ are the penetration depth, the coherence length, and the GL parameter defined in the Section I B. $\vec{A}$ and H are the vector potential and magnetic field respectively. We seek to find the solution ψ that minimizes the free energy (21).

To solve for ψ, the NGL rewrite the GL equations in the following form using the London gauge $\nabla \cdot \vec{A} = 0$. The GL equations assumes the following form:

$$\left(-i\nabla - \vec{A}\right)^2 \psi = \psi(1 - |\psi|^2), \tag{22}$$

and

$$-\kappa^2 \Delta \vec{A} = \frac{1}{2i}(\psi^* \nabla\psi - \psi\nabla\psi^*) - |\psi|^2 \vec{A}, \tag{23}$$

with the boundary condition $\vec{n} \cdot \left(-i\nabla - \vec{A}\right)\psi|_{\text{boundary}} = 0$.

Milošević's algorithm solve the two coupled GL equations for a fixed magnetic field self-consistently using the link variable approach[41]. NGL defines the link variables between $\vec{r_1}$ and $\vec{r_2}$ as

$$U_\mu^{\vec{r_1},\vec{r_2}} \equiv \exp\left[-i \int_{\vec{r_1}}^{\vec{r_2}} \vec{A_\mu}(\vec{r}) \cdot d\vec{\mu} \right], \tag{24}$$

where $\mu = x, y, z$. In NGL calculation, the whole system is discretized and mapped on a rectangular grid. After substituting equation (24) into the GL equations (22) and (23) and

perform proper transformations, the two coupled GL equations become:

$$\begin{aligned}\frac{\partial\psi}{\partial t} =&\frac{U_x^{kj}\psi_k}{a_x^2}+\frac{U_x^{ij}\psi_i}{a_x^2}+\frac{U_y^{mj}\psi_m}{a_y^2}+\frac{U_y^{nj}\psi_n}{a_y^2}\\ &-2\psi_j\left(\frac{1}{a_x^2}+\frac{1}{a_y^2}\right)-(|\psi_j|^2-1)\psi_j+\tilde{f}_j(t),\end{aligned} \tag{25}$$

and

$$-i\frac{1}{U_x^j}\nabla(U_x^j\psi_j)=-i\frac{U_x^{kj}\psi_k-\psi_j}{a_x}. \tag{26}$$

In equation (25), the different indices represent adjacent grid points to the point j and a_x, a_y, a_z are lattice constants for the grid used. For example, ψ_k represents the order parameter at grid point k. The $\tilde{f}(t)$ is a dimensionless random force.

The value of the order parameter ψ at each grid point can be solved using equation (25). The order parameter ψ will then be used to calculate the supercurrent using equation (26). Next, the NGL uses the supercurrent to update the vector potential. The vector potential is substituted back to the equation (25), and the order parameter can be calculated again. This process is repeated until a convergent solution for both GL equations is found.

After finding the order parameter ψ, we can use it to calculate the current density, phase, and the total energy of the system. The current density and the phase indicate the number of vortices and the vortex structure in the system, which is important for our study.

B. Rescaling The Coherence Length

There are several different ways to introduce anisotropy into the discrete GL equations. In this project, we introduce anisotropy into the GL equations by multiplying a rescaling constant η_x to the two link variable terms of the x direction of equation (25), i.e. the first two terms of the equation:

$$\frac{U_x^{kj}\psi_k}{a_x^2}+\frac{U_x^{ij}\psi_i}{a_x^2}\mapsto\eta_x\left(\frac{U_x^{kj}\psi_k}{a_x^2}+\frac{U_x^{ij}\psi_i}{a_x^2}\right). \tag{27}$$

We provide an intuitive justification for this approach. Comparing equation (25) with equation (22), we notice that the link variable terms correspond to the Laplacian of the order parameter ψ. Using $\psi\propto\exp(-r/\xi)$, the Laplacian is proportional to $\frac{1}{\xi^2}$. Therefore, we could view consider η_x as an rescaling coefficient for the coherence length

$$\eta_x=\frac{\xi_x^2}{\xi_y^2}, \tag{28}$$

which is analogous to the rescaling coefficient γ_x in the rescaling theory defined in equation (19). We will leave the formal proof for the future work.

After we plug equation (27) into equation (25), we solve the GL equations self-consistently to find the order parameter ψ in the presence of the anisotropic interaction. We can then calculate the current density and the phase using ψ.

C. NGL Results

In this project, we study the vortex structure under different magnetic field and anisotropy using NGL theory. We focus on the circular containers under weak fields. The field is defined in the unit of the critical field H_{c2} for the bulk superconductor:

$$H \propto \frac{1}{H_{c2}},$$

where we set $H_{c2} = \frac{2.07 \cdot 10^6}{2\pi} \frac{1}{\xi(0)}$ with $\xi(0) = 30$ nm. The η_x is defined above in equation (28). We run the calculation for three different fields $H = 30/H_{c2}, 40/H_{c2}, 50/H_{c2}$ and five different anisotropy strength $\eta_x = 1, 3, 5, 6, 9$. When $\eta_x = 1$, we recover the isotropic interaction. The calculation result is shown in Fig. 22, 23, and 24. We observe the formation of the vortex chains for all three magnetic fields when we ramp up the anisotropy from 1 to 9. This is in qualitative agreement with our simulation results using the phenomenological equation shown in Fig. 18 and the experimental observation shown in Fig. 12. We have verified our phenomenological equation calculation using NGL, and we are planning on to use NGL to verify our rescaling theory calculations as well.

V. SUMMARY

In this project, we use energy landscape calculation to survey different container shapes and different magnetic fields under different anisotropic interaction. We find that the vortices form vortex chains in the strong anisotropy regime. In the weak anisotropy regime, we find that the containers with low symmetry are best at identifying the anisotropic interaction. We observe qualitative difference in the triangular samples with eight vortices. After conducting energy landscape calculations, we perform the numerical Ginzburg-Landau calculations to verify our results. We showed the formation of vortex chains in the strong anisotropy regime. We are currently working on verifying the qualitative difference in the triangular containers.

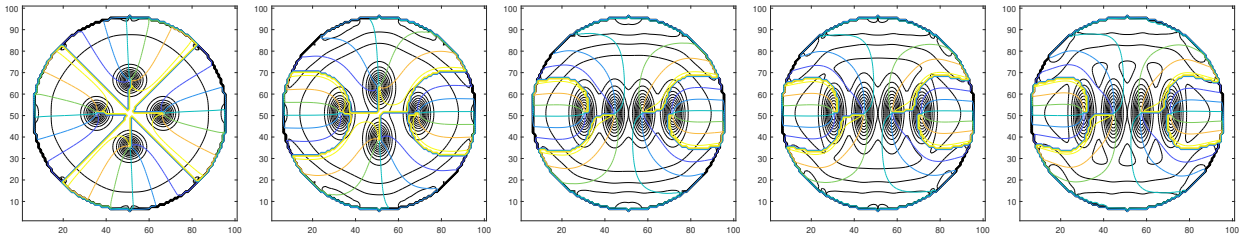

(a) $\eta_x = 1$ (b) $\eta_x = 3$ (c) $\eta_x = 5$ (d) $\eta_x = 7$ (e) $\eta_x = 9$

FIG. 22: Circular samples in the field $H = 30/H_{c2}$. The circular lines concentric to the container are contours for the density of the order parameter ψ. The lines connecting each vortices to the edge are the contours for the phases of ψ.

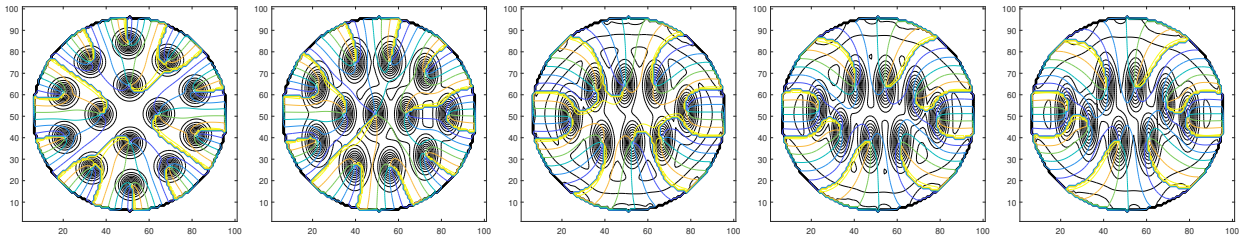

(a) $\eta_x = 1$ (b) $\eta_x = 3$ (c) $\eta_x = 5$ (d) $\eta_x = 7$ (e) $\eta_x = 9$

FIG. 23: Circular samples in the field $H = 40/H_{c2}$.

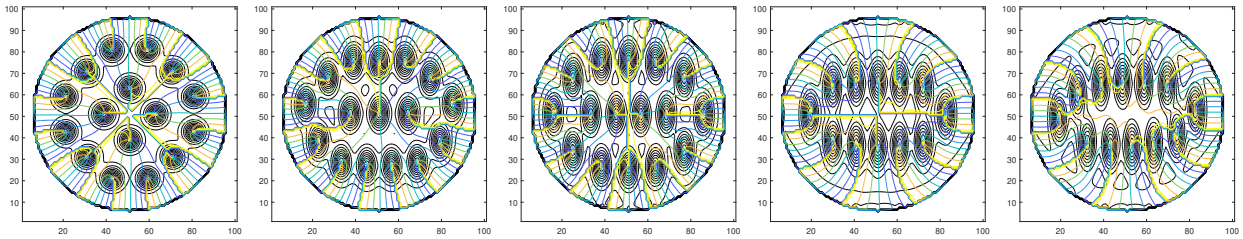

(a) $\eta_x = 1$ (b) $\eta_x = 3$ (c) $\eta_x = 5$ (d) $\eta_x = 7$ (e) $\eta_x = 9$

FIG. 24: Circular samples in the field $H = 50/H_{c2}$.

In the future, we will continue to develop the numerical Ginzburg-Landau calculations. In addition to verify the calculation results from the rescaling theory, we will also explore experimental measurements under varying magnetic fields. The vortex structure may evolve in a different way in the presence of the anisotropic interaction. The numerical Ginzburg-Landau calculation allows us to calculate how the vortex structure will vary as the applied magnetic field is changing step-wisely. We could exploit the hysteresis in the superconductors and find the experimental protocols that are best at identifying the anisotropic interaction.

VI. ACKNOWLEDGEMENTS

This thesis is dedicated to my parents. I would like to thank my family's love and support during my undergraduate years at Notre Dame. With the unconditional love from my parents, I feel that I could overcome any obstacles in my life.

I would like to thank Prof. Boldizsár Jankó for advising me on this project. I have learned habits of being a theorists from him and eventually decided to pursue a Ph.D. degree in theoretical condensed matter physics after graduation. I would like to thank Prof. Milorad Milošević for helping me understanding and using his numerical Ginzburg-Landau calculation packages. We collaborated internationally amid the tiresome COVID-19 global pandemic. I would like to thank Wenzhao Li and Dr. Xiaoyu Ma for helping me get started at using the energy landscape calculation. I would also like to thank Sushrut Ghonge and Shubin Zhang who both give valuable comments in our group meeting. I have learned a lot from them both professionally and personally.

I would also like to thank Prof. Tan Ahn, whom I conducted my first college-level physics research with, for leading me onto the path of becoming a researcher. I would like to thank Prof. Mark A. Caprio for teaching me numerical techniques and cultivating my mathematical intuitions. I want to thank Dr. Chao Yang for guiding me during the 2019 and 2020 summer, where I solidified my commitment to become a theoretical physicist in the future.

Finally, I would like to thank Yuanchen Li, Gelin Li, Jiaxuan Ren, Miaochen Jin, Emilia Wang, Chang Zhou, Zhuoran Han, Wenyi Wu, and all my other friends. They keep my company, cheer me up, and support me during the down times in the past four years. I feel lucky for having them in my life, and we shall be friends forever.

---

[1] M. Tinkham, *Introduction to Superconductivity: Second Edition (Dover Books on Physics) (Vol i)*, 2nd ed. (Dover Publications, 2004).

[2] W. Meissner and R. Ochsenfeld, Ein neuer Effekt bei Eintritt der Supraleitfähigkeit, Naturwissenschaften **21**, 787 (1933).

[3] J. W. Rohlf, *Modern physics from alpha to Z°* (John Wiley, 1994).

[4] Phase diagram, http://www.futurescience.com/manual/phase.gif.

[5] J. Bardeen, L. N. Cooper, and J. R. Schrieffer, Theory of Superconductivity, Physical Review

108, 1175 (1957).

[6] V. L. Ginzburg and L. D. Landau, On the Theory of superconductivity, Zh. Eksp. Teor. Fiz. **20**, 1064 (1950).

[7] S. J. Bending and M. J. W. Dodgson, Vortex chains in anisotropic superconductors, Journal of Physics: Condensed Matter **17**, R955 (2005).

[8] G. R. Stewart, Unconventional superconductivity, Advances in Physics **66**, 75 (2017).

[9] The magnetic properties of superconducting alloys, Journal of Physics and Chemistry of Solids **2**, 199 (1957).

[10] Mise en evidence par diffraction de neutrons d'une structure periodique du champ magnetique dans le niobium supraconducteur, Physics Letters **9**, 106 (1964).

[11] The direct observation of individual flux lines in type II superconductors, Physics Letters A **24**, 526 (1967).

[12] R. P. Huebener, The Abrikosov Vortex Lattice: Its Discovery and Impact, Journal of Superconductivity and Novel Magnetism **32**, 475 (2019).

[13] G. Blatter, Vortex matter, Physica C: Superconductivity Materials and Mechanisms of Superconductivity High Temperature Superconductors V, **282-287**, 19 (1997).

[14] F. Steglich, J. Aarts, C. D. Bredl, W. Lieke, D. Meschede, W. Franz, and H. Schäfer, Superconductivity in the Presence of Strong Pauli Paramagnetism: Ce${\mathrm{Cu}}_{2}$${\mathrm{Si}}_{2}$, Physical Review Letters **43**, 1892 (1979).

[15] T. Cren, L. Serrier-Garcia, F. Debontridder, and D. Roditchev, Vortex Fusion and Giant Vortex States in Confined Superconducting Condensates, Physical Review Letters **107**, 097202 (2011).

[16] L. F. Chibotaru and V. H. Dao, Stable fractional flux vortices in mesoscopic superconductors, Physical Review B **81**, 020502 (2010).

[17] F. W. J. Hekking, L. I. Glazman, K. A. Matveev, and R. I. Shekhter, Coulomb blockade of two-electron tunneling, Physical Review Letters **70**, 4138 (1993).

[18] I. V. Grigorieva, W. Escoffier, J. Richardson, L. Y. Vinnikov, S. Dubonos, and V. Oboznov, Direct Observation of Vortex Shells and Magic Numbers in Mesoscopic Superconducting Disks, Physical Review Letters **96**, 077005 (2006).

[19] L. Y. Vinnikov, J. Karpinski, S. M. Kazakov, J. Jun, J. Anderegg, S. L. Bud'ko, and P. C. Canfield, Vortex structure in $\mathrmMgB_2$ single crystals observed by the Bitter decoration technique, Phys. Rev. B **67**, 092512 (2003).

[20] X. Yang, Z. Du, H. Lin, D. Fang, H. Yang, X. Zhu, and H.-H. Wen, Vortex lattice and vortex bound states in ${\mathrm{CsFe}}_{2}{\mathrm{As}}_{2}$ investigated by scanning tunneling microscopy/spectroscopy, Physical Review B **98**, 024505 (2018).

[21] R. Heeb and D. F. Agterberg, Ginzburg-Landau theory for a p -wave Sr 2 RuO 4 superconductor: Vortex core structure and extended London theory, Physical Review B **59**, 7076 (1999).

[22] S. J. Bending, Scanning Hall probe microscopy of vortex matter, Physica C: Superconductivity Vortex Matter in Nanostructured Superconductors, **470**, 754 (2010).

[23] I. V. Grigorieva, Magnetic flux decoration of type-II superconductors, Superconductor Science and Technology **7**, 161 (1994).

[24] A. Grigorenko, S. Bending, T. Tamegai, S. Ooi, and M. Henini, A one-dimensional chain state of vortex matter, Nature **414**, 728 (2001).

[25] H. J. Zhao, V. R. Misko, F. M. Peeters, S. Dubonos, V. Oboznov, and I. V. Grigorieva, Vortex configurations in mesoscopic superconducting triangles: Finite-size and shape effects, EPL (Europhysics Letters) **83**, 17008 (2008).

[26] H. J. Zhao, V. R. Misko, F. M. Peeters, V. Oboznov, S. V. Dubonos, and I. V. Grigorieva, Vortex states in mesoscopic superconducting squares: Formation of vortex shells, Physical Review B **78**, 104517 (2008).

[27] G. C. Ménard, S. Guissart, C. Brun, R. T. Leriche, M. Trif, F. Debontridder, D. Demaille, D. Roditchev, P. Simon, and T. Cren, Two-dimensional topological superconductivity in Pb/Co/Si(111), Nature Communications **8**, 2040 (2017).

[28] K. Budde, E. Abram, V. Yeh, and M. C. Tringides, Uniform, self-organized, seven-step height $\mathrm{P}\mathrm{b}/\mathrm{S}\mathrm{i}(111)\ensuremath{-}(7\ifmmode\times\else\texttimes\fi{}7)$ islands at low temperatures, Physical Review B **61**, R10602 (2000).

[29] H.-J. Kim, B. Kang, H.-S. Lee, and S.-I. Lee, Measurement of the anisotropy ratios in MgB2 single crystals, Physica B: Condensed Matter Proceedings of the International Conference on Strongly Correlated Electron Systems, **378-380**, 890 (2006).

[30] D. A. Wollman, D. J. Van Harlingen, W. C. Lee, D. M. Ginsberg, and A. J. Leggett, Experimental determination of the superconducting pairing state in YBCO from the phase coherence of YBCO-Pb dc SQUIDs, Physical Review Letters **71**, 2134 (1993).

[31] M. V. Milošević and R. Geurts, The Ginzburg–Landau theory in application, Physica C: Superconductivity Vortex Matter in Nanostructured Superconductors, **470**, 791 (2010).

[32] D. A. Evans and D. J. Wales, The free energy landscape and dynamics of met-enkephalin, The Journal of Chemical Physics **119**, 9947 (2003).

[33] D. J. Wales, Energy landscapes: Calculating pathways and rates, International Reviews in Physical Chemistry **25**, 237 (2006).

[34] N. J. Giordano and H. Nakanishi, *Computational Physics*, 2nd ed. (Pearson/Prentice Hall, Upper Saddle River, NJ, 2006).

[35] Q-Chem 4.3 User's Manual : Eigenvector-Following (EF) Algorithm, https://manual.q-chem.com/4.3/sect-ef.html.

[36] J. Baker, An algorithm for the location of transition states, Journal of Computational Chemistry **7**, 385 (1986).

[37] A. Banerjee, N. Adams, J. Simons, and R. Shepard, Search for stationary points on surfaces, The Journal of Physical Chemistry **89**, 52 (1985).

[38] M. W. Olszewski, M. R. Eskildsen, C. Reichhardt, and C. J. O. Reichhardt, Structural transitions in vortex systems with anisotropic interactions, New Journal of Physics **20**, 023005 (2018).

[39] G. Blatter, V. B. Geshkenbein, and A. I. Larkin, From isotropic to anisotropic superconductors: A scaling approach, Physical Review Letters **68**, 875 (1992).

[40] V. A. Schweigert and F. M. Peeters, Phase transitions in thin mesoscopic superconducting disks, Physical Review B **57**, 13817 (1998).

[41] R. Kato, Y. Enomoto, and S. Maekawa, Effects of the surface boundary on the magnetization process in type-II superconductors, Physical Review B **47**, 8016 (1993).